Catalysis Science & Technology

Accepted Manuscript

ROYAL SOCIETY OF CHEMISTRY

www.rsc.org/catalysis

Varying the oxidative environment causes phase changes in the catalyst which influence the product selectivity of octane activation.

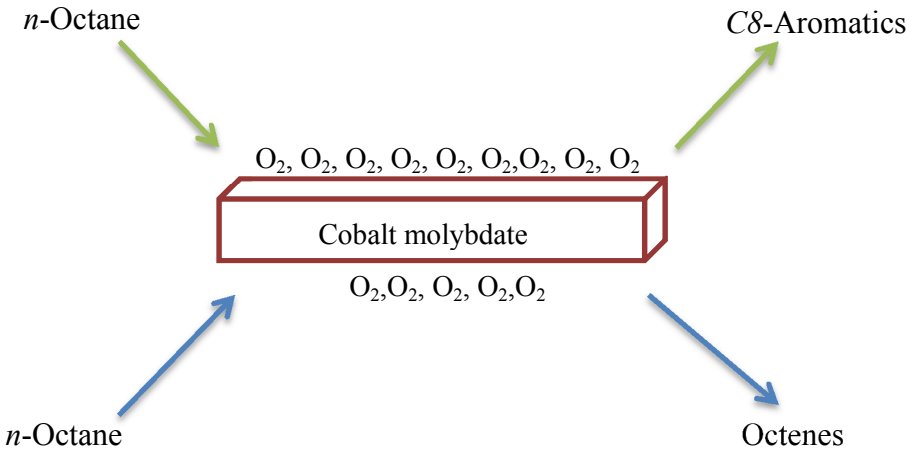

Cite this: DOI: 10.1039/c0xx00000x

www.rsc.org/xxxxxx

ARTICLE TYPE

The effect of the oxidation environment on the activity and selectivity to aromatics and octenes over cobalt molybdate in the oxidative dehydrogenation of *n*-octane

Mohamed I. Fadlalla[a] and Holger B. Friedrich[a]*

Received (in XXX, XXX) Xth XXXXXXXXX 20XX, Accepted Xth XXXXXXXXX 20XX
DOI: 10.1039/b000000x

A cobalt molybdate catalyst was synthesised by the co-precipitation method and characterized by XRD, BET-surface area measurements, ICP-OES, Raman, TPR, TPO, SEM and SEM-EDX. XRD results showed that the dominate phase in the catalyst is the β-phase. The ratio of Co:Mo was determined by ICP-OES to be 1:1.04. The excess molybdenum is found in the molybdenum trioxide phase as shown by the Raman results. The TPR/O/R/O/R results showed that the catalyst can undergo the redox cycle where cobalt molybdate reduces to the molybdite and spinel form of cobalt molybdate (by 5% hydrogen) and oxidize back to the cobalt molybdate after oxygen exposure. The catalytic testing was carried out in a continuous flow fixed bed reactor at atmospheric pressure and a temperature range of 350 to 550 °C in 50 °C intervals with different oxygen content (*i.e.* C:O ratio of 8:0, 8:1, 8:2, 8:3 and 8:4) in the reaction mixture. The conversion of *n*-octane increased with increase in the oxygen content in the reaction mixture, which was accompanied by changes in the selectivity patterns. The dominant products were the octenes and COx at all temperatures and different carbon to oxygen ratios. Furthermore, the selectivity to aromatic products increased with increase in the strength of the oxidising environment in the feed mixture and was dominated by styrene and ethylbenzene (both products of 1,6-cyclization). The yields of octenes, aromatics, cracked products and COx at 500 °C showed that an increase in the oxygen content resulted in a decrease in the yield to octenes and an increase in what can be considered secondary products (*i.e.* aromatics and COx). The total selectivity percentage of value-added products (*i.e*. octenes and aromatics) also decreased with increase in the oxygen content, due to the increase in cracked products and COx yields (which are not considered value added products). Characterization of the spent catalysts at the different conditions showed that the catalyst maintains the cobalt molybdate phase under the 8:2, 8:3 and 8:4 C:O conditions, while complete segregation took place under dehydrogenation conditions and partial segregation occurred at an 8:1 C:O ratio.

.

1 Introduction

Alkenes have been produced by dehydrogenation for the past six decades, and have large scale applications in the petrochemical industry. They are used as feedstock in the production of value added products (though functionalization) [1, 2]. In recent years, the petrochemical industry has looked towards using paraffins to produce value-added products through oxidative dehydrogenation or partial oxidation of paraffins, since paraffins are abundant and cheap, in part due to the increase in the number of the coal to liquid and gas to liquid plants (CTL and GTL) worldwide [3]. Oxidative dehydrogenation of paraffins offers a number of advantages, namely; the reaction is exothermic, low energy costs, low environmental impact, lower greenhouse gas emissions [3] and it does not suffer from equilibrium limitation. Moreover, dehydrogenation of alkanes is accompanied by low selectivities and high yields of coke and cracked products, moreover, carbon deposit results in blockage of the active site in the catalyst leading to a shorting of the life span of the catalyst [4]. The use of oxygen in the reaction mixture reduces coke formation and overcomes equilibrium and thermodynamic limitations of the dehydrogenation reaction [1, 5, 6]. Therefore, activation of paraffins via oxidative dehydrogenation is gaining a lot of interest academically and industrially [7, 8].

Molybdates are considered one of the better catalysts for the oxidation of olefins due to their suitable solid-state redox [9-15]. Furthermore, the advantage of molybdates is that the metal-oxygen bond can be tailored, based on the structure and the nature of the molybdate [16]. It has been shown that the different phases (*i.e.* α and β) nickel molybdate have different activity and selectivity to hexenes in the oxidative dehydrogenation of *n*-

hexane [3]. Also the effect of carbon to oxygen ratio affects the selectivity to hexenes over the β-nickel molybdate [17].

Cobalt molybdate has been used in different types of catalysis such as hydrodesulfurization [18], hydrolysis of carbonyl sulphide COS [19] and the oxidative dehydrogenation of light paraffins, mainly propane [20-23]. For the latter processes selectivity to useful products was 64% at 7% conversion of propane, however, an increase in the conversion to 15% resulted in a decrease in the selectivity to useful products [23]. Moreover, cobalt molybdate showed good activity and selectivity to propene among different molybdates studied, such as Cu, Fe, Mn and Zn [20-22].

Based on the activity and selectivity of cobalt molybdate in the oxidative dehydrogenation of light paraffins and the increase in the amount of *n*-octane worldwide, we decided to investigate the activity and selectivity of cobalt molybdate in the oxidative dehydrogenation of *n*-octane. In addition, the effect of the carbon to oxygen ratio on the catalyst activity, selectivity and stability was explored.

2 Experimental

2.1 Catalyst synthesis

The cobalt molybdate catalyst was prepared by the co-precipitation method modified from literature [21]. Equi-concentration solutions of molybdenum ($(NH_4)Mo_7O_{24}.4H_2O$, Merck) and cobalt ($Co(NO_3)_2.6H_2O$), ACE) were prepared with deionized water. The molybdenum solution was stirred at room temperature and the pH was adjusted to 6 using aqueous ammonia (Saarchem). Then the cobalt solution was added drop-wise with continuous stirring. Upon addition of the cobalt solution the mixture turned purple. After complete addition of the cobalt solution, the mixture was heated to 90 °C. Once part of the water had evaporated a purple precipitate formed. The slurry was then dried in an oven for 12 hours at 110 °C. The purple precipitate was calcined at 550 °C for 2 hours to produce cobalt molybdate.

2.2 Catalyst characterization

The phase composition of the catalyst was analysed by X-Ray diffraction using a Bruker D8 Advance operated with a copper radiation source (1.5406 λ wavelength) and an Anton Paar XRK 900 reaction chamber. BET-surface area measurements were carried out after the sample was degassed at 200 °C overnight under nitrogen flow using a Micromeritics flow prep 060 and analysed using a Micromeritics Tristar II. The Raman analyses were carried out using an Advantage 532 series spectrometer with Nuspec software. The molar ratio of the two metals (*i.e.* cobalt and molybdenum) in the bulk of the catalyst was determined by inductively coupled plasma-optical emission spectroscopy (ICP-OES) using a PerkinElmer Precisely Optima 5300DV, after the sample was digested using hydrochloric acid (HCl 32%, Merck). Temperature programme reduction (TPR), temperature programme desorption (TPD) and temperature programmed reduction/oxidation/reduction (TPR/O/R/O/|R) were carried out in a Micromeritics 2920 Autochem II chemisorption analyser following a reported method [1]. The catalyst structure and surface morphology were viewed using a Ziess Ultra Plus scanning electron microscope. Samples were placed on aluminium stubs using a double sided carbon tape and the samples were coated with carbon.

2.3 Catalytic testing

The catalytic testing was carried out using a continuous flow fixed bed reactor in vertical flow mode. The catalyst was placed in the middle of the isothermal region in the stainless steel tube (10 mm ID and 210 mm length). All voids in the reactor tube were filled with carborandum (24 gritt, Polychem). 1 ml (0.8091 g) of the catalyst was freshly used for each reaction, with a particle size between 1000-600 µm. All reactions were carried out in the temperature range of 350 – 550 °C at 50 °C intervals. The molar ratio of carbon to oxygen was adjusted to obtain the different C:O ratios (*i.e.* 8:1, 8:2, 8:3 and 8:4) using air as the oxygen source. The target GHSV of 4000 h^{-1} (total flow of gases 67 ml/min) was obtained by using nitrogen as diluent inert gas. All liquids (unreacted octane and products) were collected in a catch-pot that is cooled to 2 °C. The volume of the gaseous products were measured using a Ritter Drum-Type gas flow meter.

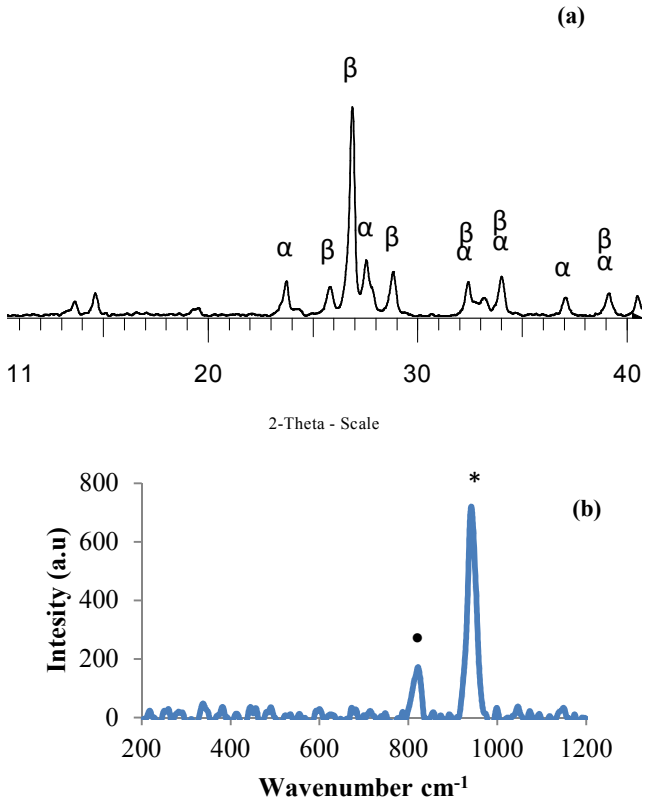

Fig1: XRD pattern (a) of the cobalt molybdate catalyst synthesised by co-precipitation (α and β cobalt molybdate phases and only the major peaks are labelled) and Raman spectrum (b) cobalt oxide (•) and cobalt molybdate (*)

All the reaction products (liquid and gas) were identified and quantified using gas chromatography (GC). The gaseous products were injected into a PerkinElmer Clarus 400 equipped with a TCD detector (COx analysis) and also in a PerkinElmer Clarus 400 equipped with a FID detector. The liquid products from the catch-pot were analysised by the GC with the FID detector. All reactions reported have a carbon balance between

95-105% and the results reported are the average of at least two runs.

2.4 Spent catalyst characterization

The used catalyst was kept under nitrogen after the reaction and characterized by XRD, BET-surface area measurements and Raman spectroscopy as described in Section 2.2.

3 Results and discussion

3.1 Catalyst characterization

The X-Ray diffraction results (Fig. 1 a) showed the two phases of the cobalt molybdate present, which are the α- and β-$CoMoO_4$. The main difference between these two phases is in the co-ordination environment around the molybdenum center. The co-ordination around the molybdenum centre in β-$CoMoO_4$ is partially distorted tetrahedral, while in the α-$CoMoO_4$ phase the co-ordination is octahedral around the molybdenum centre [24]. They also differ in colour is the physical appearance, where the former is purple in colour and the latter is green. The transformation between the two phases can be achieved by applying pressure or increasing the temperature. The dominance of the β-phase at room temperature is expected, since that phase is the more stable form of $CoMoO_4$ at room temperature and atmospheric pressure [24].

The Raman analysis (Fig. 1 b) showed two peaks at 940 cm^{-1} and 818 cm^{-1}. The peak at 940 cm^{-1} corresponds to the cobalt molybdate phase, in particular the β-form of cobalt molybdate [25]. Thus, these results relate well with the XRD results showing that the β-$CoMoO_4$ is the dominant phase. Moreover, the expected Raman peak for the α-$CoMoO_4$ (at 950 cm^{-1}) was not clearly observed. However, the broadening of the peak at 940 cm^{-1} suggested that the peak due to α-$CoMoO_4$ could be overlapping with the characteristic peak of the β- $CoMoO_4$. The presence of MoO_3 was indicated by the Raman peak at 818 cm^{-1}, which corresponds to the Mo-O asymmetric frequency [26]. The presence of the excess molybdenum (likely in the form of MoO_3) was also detected by ICP-OES which gave a Co:Mo ratio of 1:1.04. The surface area of the material was 12 m^2/g, which is in the normal range for molybdates [21].

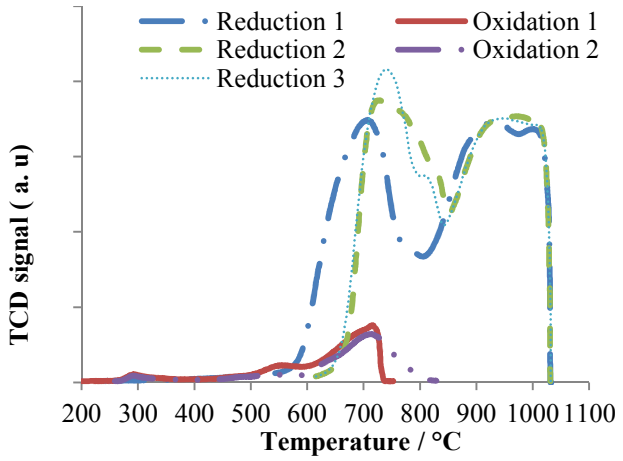

Fig. 2: TPR/O/R/O/R of the cobalt molybdate catalyst synthesised by the co-precipitation method.

The temperature programmed reduction, oxidation and repeat cycles of reduction and oxidation (Fig. 2) showed two reduction peaks (Fig. 2, reduction 1), the first peak at around 650 °C, the second peak at around 850 °C. The lower temperature reduction peak is due to the reduction of cobalt molybdate to molybdite ($Co_2Mo_3O_8$) and the spinel form of cobalt molybdate (Co_2MoO_4), both present in equimolar quantities [27]. The higher temperature reduction peak is due to complete reduction of molybdite and the spinel to the metal form (*i.e.* cobalt and molybdenum) [27]. Also, the small quantity of molybdenum trioxide present is likely reducing to the molybdenum dioxide phase at around 650 °C [27]. Furthermore, the reduction-oxidation-reduction-oxidation-reduction cycle shows that the catalyst can go through the redox cycle without permanently changing phase, *i.e.* as long as there is enough oxygen to oxidize the catalyst back to the cobalt molybdate phase, phase segregation does not take place.

The surface morphology of the catalyst (S 1) was observed by SEM. The results showed that the catalyst consists of round shaped particles and some plate like particles. The plate like particles are believed to be due to the free molybdenum trioxide that is present in the catalyst in small quantity and the round particles are the cobalt molybdate. This also would agree with the Raman results, since this shows that the catalyst is dominated by the cobalt molybdate phase.

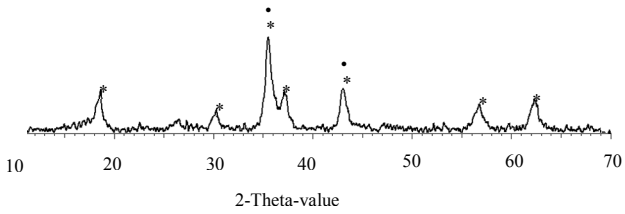

Fig. 3: XRD diffractogram of the used catalyst under *n*-octane at an 8:0 C:O ratio at 4000 h^{-1} showing Co_3O_4 (*) and MoO_2 (•).

3.2 Catalytic results

3.2.1 Octane activation at a C:O ratio of 8:0 (dehydrogenation)

There was low conversion of *n*-octane over cobalt molybdate under reducing conditions (no oxygen), with a highest conversion of 11% at 550 °C. The low conversion could be attributed to the equilibrium of the reaction not being pushed towards product formation due to the absence of the formation of the thermodynamically stable products (such as COx and water) [28]. Furthermore and/or in addition, the strong reducing environment resulted in reduction of the catalyst, since there is not sufficient lattice oxygen to maintain the initial phase of the catalyst. This was confirmed by the spent catalyst characterization, where the XRD of the spent catalyst (Fig. 3) showed the formation of cobalt oxide and molybdenum oxide. These phases are the same phases that were found to form in the TPR analysis of cobalt molybdate.

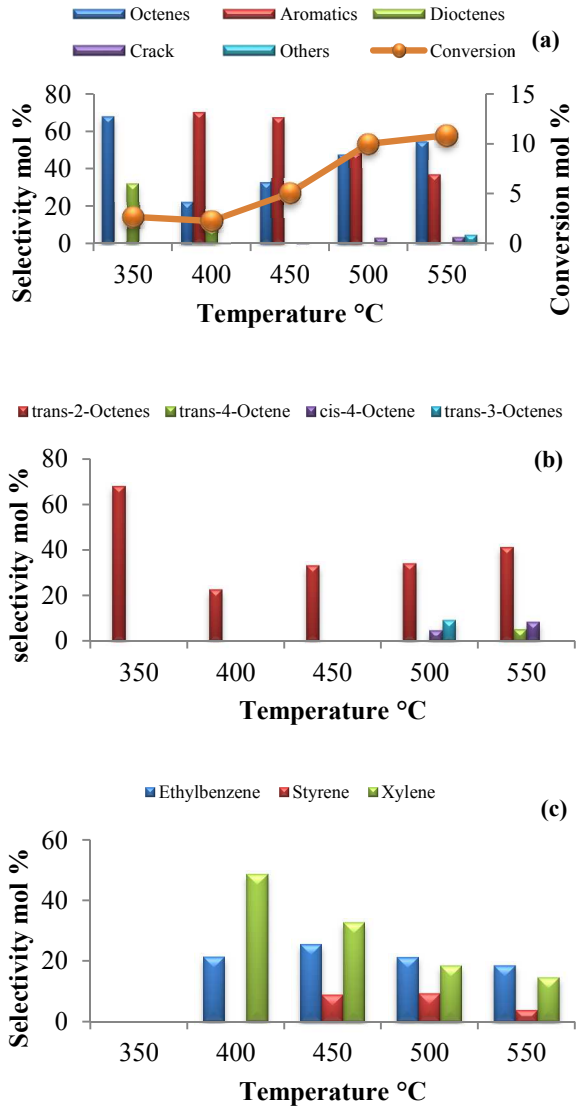

Fig. 4: Conversion and general selectivity pattern (a), octenes (b) and aromatics selectivity breakdown (c) of cobalt molybdate under *n*-octane at an 8:0 C:O ratio at 4000 h^{-1}

The Raman analysis (S 2) confirmed the formation of the cobalt oxide. At 350 °C the only products observed were the dehydrogenation products (*i.e.* octenes and octadienes). As the reaction temperature increased (400-450 °C), the selectivity to the dehydrogenation products decreased and the selectivity to the dehydrocyclization products (aromatization) increased. This change occurs at the onset reduction temperature of molybdenum trioxide as observed in the TPR profile. However, at the onset temperature for the reduction of cobalt molybdate (~ 500 °C) the catalyst again favoured dehydrogenation only, rather than the dehydrocyclization path, as demonstrated by the increase in selectivity to the octenes and decrease in the selectivity to the aromatics (Fig. 4 a).

The breakdown of the octenes selectivity (Fig. 4 b) shows the dominance of the 2-octene isomer, that is accompanied by o-xylene dominating in the aromatic product breakdown (Fig. 4 c). This correlation suggests that 2-octene is the precursor to xylene through 2,7-cyclization. There was no 1-octene observed at the different temperatures, however, ethylbenzene and styrene were detected at 400 °C and 450 °C, respectively. This could be attributed to the high reactivity of 1-octene, which can be explained by the fact that 1-octene contains six sp^3 carbon atoms in a sequence providing the free rotation that is required for 1,6 cyclization to take place leading to the formation of ethylbenzene and styrene [28-31]. At higher temperatures the other octenes isomers (*i.e.* 3 and 4-octenes) were detected with low selectivities.

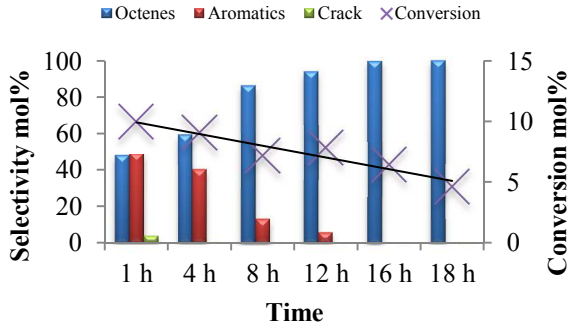

Fig. 5: Cobalt molybdate catalyst activity and selectivity as function of time in the dehydrogenation of *n*-octane at 4000 h^{-1} and 500 °C.

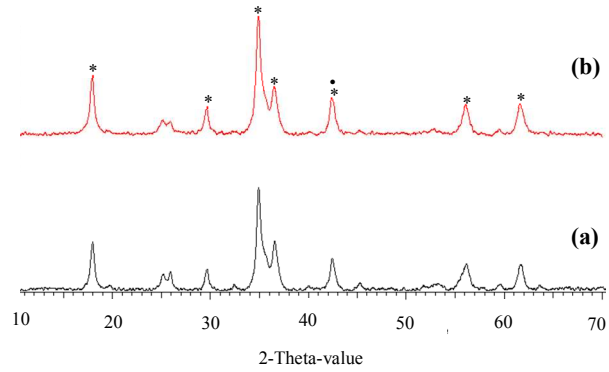

Fig. 6: XRD patterns for the used catalyst under dehydrogenation conditions at 500 °C and 4000 h^{-1} after 4 hours (a) and 18 hours (b) reaction. The two phases detected were Co_3O_4 (*) and MoO_2 (•).

A time on stream experiment was carried to study the stability of the catalyst under dehydrogenation conditions at 500 °C. Fig. 5 shows the catalyst activity and selectivity to octenes and aromatics. Reaction time has clear effects on both catalyst activity and selectivity. As the conversion of n-octane decreased with time so too did the aromatics selectivity. The selectivity to octenes increased as the selectivity to aromatics decreased. This is likely due to the stripping of the lattice oxygen from the catalyst that is required for the aromatization of the octenes products to produce aromatics. The catalyst was removed and characterized, once after 4 hours and again in a repeat run after 18 hours on stream to investigate any changes in the catalyst. Fig. 6 shows the XRD pattern of the used catalyst. The cobalt molybdate has been reduced to the oxide forms of cobalt and molybdenum. Thus, the change in the catalyst activity and selectivity is likely due to phase changes in the catalyst brought upon by the strong reducing environment. Furthermore, the

change in the catalyst structure, activity and selectivity indicates that the reaction, at least in part, goes through the oxidative dehydrogenation pathway rather than the dehydrogenation pathway.

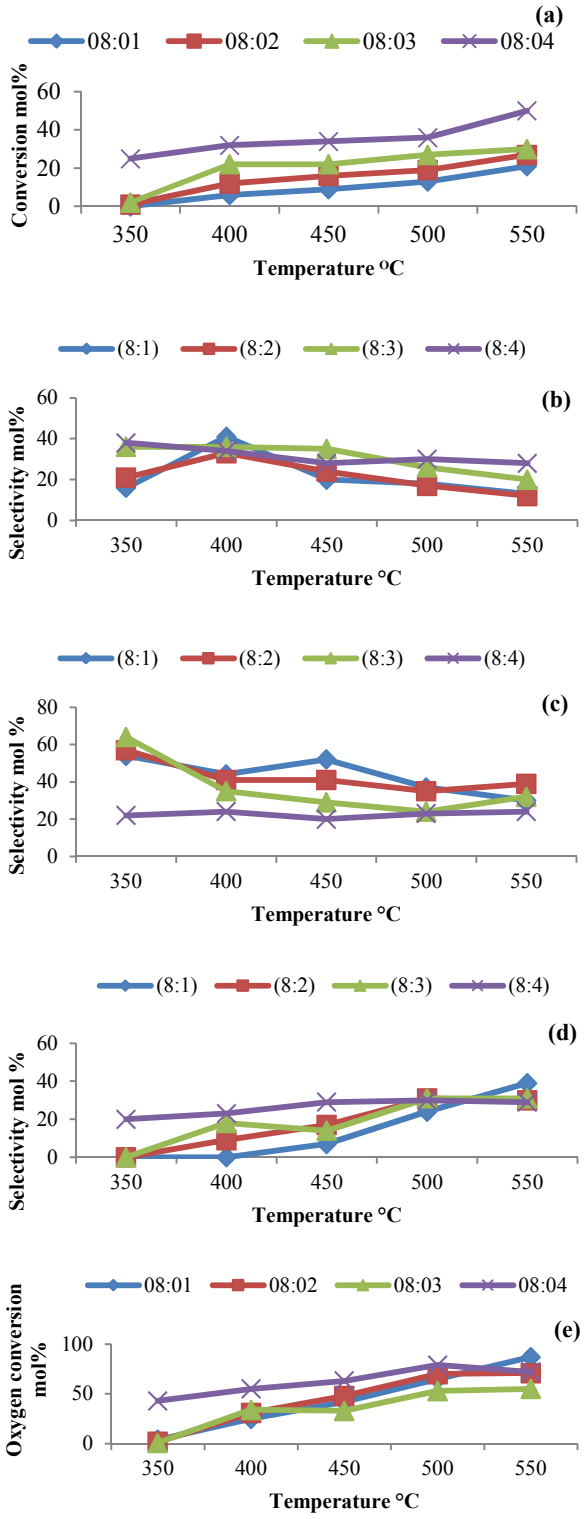

Fig. 7: Effect of oxygen on the conversion of *n*-octane (a), COx selectivity (b), octenes selectivity (c), aromatics selectivity (d) and oxygen conversion over cobalt molybdate at 4000 h^{-1} as function of reaction temperature.

3.2.2 Effect of oxygen content on activity and selectivity

Four different carbon to oxygen (C:O) ratios were investigated to shed light on their effect on the conversion and the selectivity of the cobalt molybdate to non-COx products. As the oxygen content in the reaction mixture increased in the order 8:1< 8:2< 8:3< 8:4, so did the conversion of *n*-octane (Fig. 7 a). The *iso*-thermal increase, with increasing oxygen concentration, in the conversion is due to the shift in the reaction equilibrium towards the products, which is brought on by the increase in the formation of COx (Fig. 7 b) and water as a function of oxygen in the reaction mixture [28]. The highest selectivity to COx was obtained at 400 °C with a carbon to oxygen ratio of 8:1 (oxygen deficient environment), after which the selectivity decreased with increasing temperature to the lowest COx selectivity among the different carbon to oxygen ratios. A similar pattern was observed for the carbon to oxygen ratio of 8:2, however, the increase at 400 °C was lower in comparison to that at the 8:1 ratio. The selectivity to COx generally decreased with an increase in the reaction temperature, as a result of the formation of more ODH products. The selectivity to octenes in general increased with a decrease in the oxygen content in the reaction mixture. At low oxygen content (*i.e.* C:O ratio of 8:1 and 8:2) the formation of octenes was favoured and became less favoured with higher oxygen content (*i.e.* 8:3 and 8:4) due to secondary reactions [28-32]. Moreover, the selectivity to octenes (Fig. 7 c) decreased or reached a plateau at higher temperatures due to subsequent reactions forming aromatics and cracked products. The increase in the selectivity towards aromatics at high temperatures (Fig. 7 d) supports the belief that octenes are the precursors to aromatics through cyclization.

The dominant octene isomer is 2-octene (as in the dehydrogenation reaction) across the different temperatures and carbon to oxygen ratios. However, as the oxygen content increased in the reaction mixture other isomers were formed (*i.e.* 3- and 4-octenes), though their selectivities remained lower than that to 2-octene. With regards to the aromatics breakdown, the selectivity to xylene was the highest under oxygen deficient environment conditions (*i.e.* 8:1), however, an increase in oxygen content in the reaction mixture favoured the formation of ethylbenzene and, more so, styrene (*i.e.* products of 1,6-cyclization).

The increase in the selectivity to ethylbenzene and styrene can be attributed to the increase in the oxygen available for the 1,6-cyclization and dehydrogenation to give styrene. The increase in the 1,6-cyclization was accompanied by a decrease in the selectivity to 1-octene, which is believed to be the precursor for the 1,6-cyclization. This hypothesis was supported by the increase in the selectivity toward 4-octene relative to the other octenes in oxygen rich environments, since its less reactive than the other isomers and the position of the double bond hinders cyclization. The general trend observed for oxygen conversion over cobalt molybdate (Fig. 7 e) is that the conversion increased as the reaction temperature increased, consequently, the *n*-octane conversion also increased. Selectivity to COx and aromatics plateaued at 500 and 550 °C, the conversion of oxygen also generally plateaued at the same temperatures indicating the correlation between oxygen and formation of those products. This trend was also observed in the ODH of *n*-octane over

Co/ceria [33] and vanadium [28] based catalysts. At 550 °C and a C:O ratio of 8:1 the selectivity to aromatics increased and that was accompanied by an increase in the oxygen conversion, which indicates that oxygen has been consumed to produce aromatics. Furthermore, the results obtained showed that the system is always oxygen sufficient and at no temperature or C:O ratio was the system oxygen deficient. Furthermore, the ratio of CO and CO_2 was constant at all ratios (S 3), which indicates that CO does not undergo deep oxidation to form CO_2 [34].

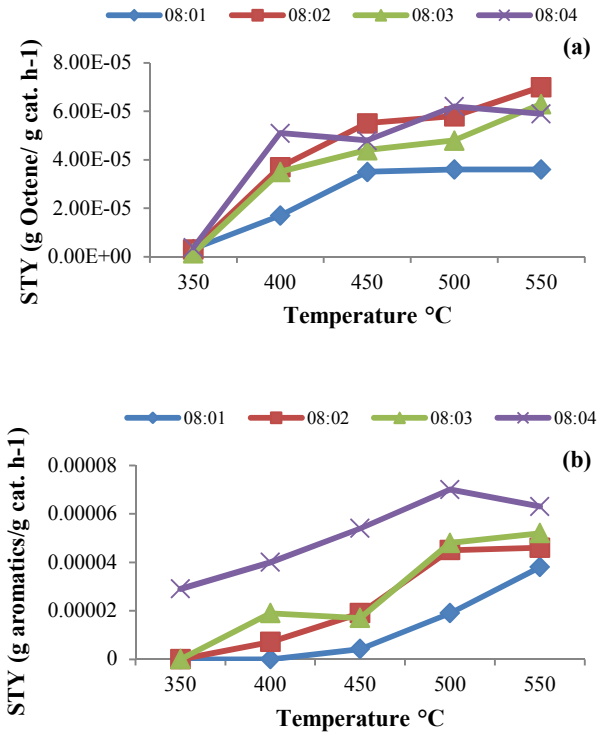

Fig. 8: Formation rate of octenes (a) and aromatics (b) as a function of oxygen concentration and reaction temperature in ODH of n-octane over cobalt molybdate.

A further way to investigate the effect of both oxygen concentration and reaction temperature on the reaction is by determining the formation rate of value added products (*i.e.* octenes and aromatics). The formation rate of octenes (Fig. 8 a) and aromatics (Fig. 8 b) were calculated as reported by Solsona *et al.* [34]. The general trend in the formation rate of octenes (Fig. 8 a) is an increase in the formation rate of octenes as the oxygen concentration in the feed increased, the exception is the 8:2 C:O ratio, which showed the highest formation rate. The increase in the oxygen concentration was also accompanied by an increase in the formation rate of C8 aromatics (Fig. 8 b). This indicates that aromatics are formed through subsequent reactions starting from octene, through cyclization and dehydrogenation where oxygen is required [28, 35].

3.2.3 Effect of C:O ratio on product distribution

The yields of octenes, aromatics and COx at 500 °C as a function of the oxygen content in the reaction mixture are shown in Fig. 9 a. The yields of the octenes in general decrease slightly with increase in the oxygen content in the reaction, since these are the reagent for the formation of the secondary products (*i.e.* aromatics, cracked products and COx). This is indicated by the increase in the yield of the secondary products as the oxygen content increased. The increase in the COx yield could be as a direct result of the increase in the oxygen content causing over oxidation of octenes to the thermodynamically stable COx products. The value-added C8 selectivity % (VAP%) (Fig. 9 b) decreased with increase in the oxygen content in the reaction. This observation emphasises that the yield of undesired products (mainly COx) increased with oxygen content. At lower oxygen content (*i.e.* C:O ratios of 8:1 and 8:2) the VAP% was mainly due to the high selectivity to octenes, as the oxygen content increased so did the contribution from the aromatics to the VAP%. Thus, the ratio of 8:3 can be considered ideal for obtaining both octenes and aromatics and a lower ratio (*i.e* 8:2) is best for octenes formation.

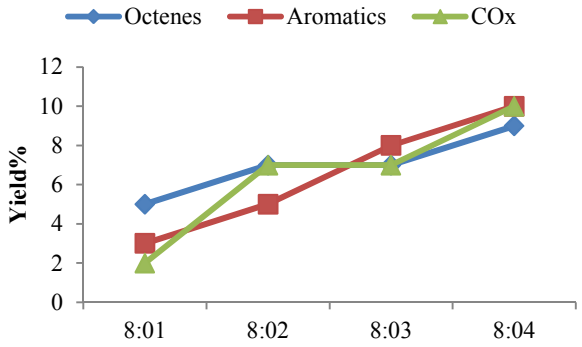

Fig. 9a: Yield % of octene, aromatics and COx products at 500 °C as function of the oxygen content in the reaction mixture.

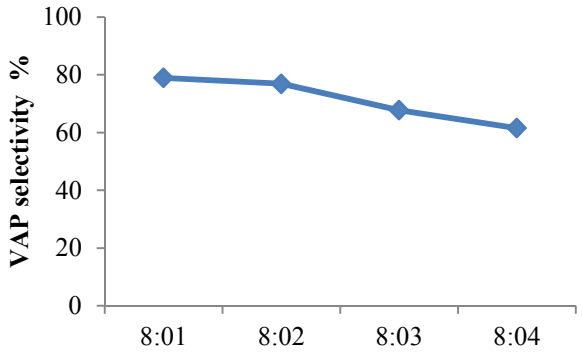

Fig. 9b: VAP% plot as effect of oxygen content over cobalt molybdate catalyst at 500 °C and GHSV of 4000 h^{-1}

3.3 Used catalyst characterization

The used catalyst was characterized using XRD, Raman and BET surface area measurements, in order to investigate any phase change that may have been brought on by the reaction conditions. Therefore, the catalyst was characterized without any pre-treatment to avoid any changes to the used catalyst. The XRD (S 3) confirms the presence of cobalt molybdate as the dominant phase in the used catalyst regardless of the oxygen content in the reaction mixture. However, the Raman analyses (Fig. 10)

showed more clearly the effect of the oxygen content in the reaction mixture. For the catalyst under oxygen deficient conditions (*i.e.* an 8:1 C:O ratio) a peak at ~ 468 cm^{-1} was detected.

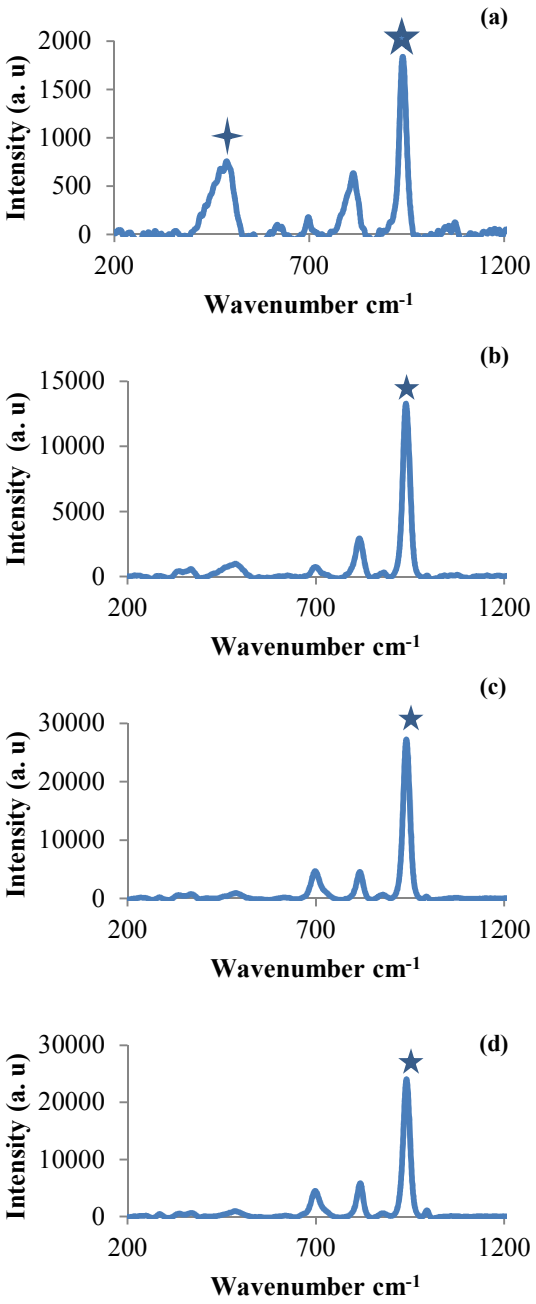

Fig. 10: Raman spectra of the used catalysts tested under different oxygen contents (a) 8:1, (b) 8:2, (c) 8:3 and (d) 8:4. Cobalt oxide(✦) and cobalt molybdate (★).

(Fig. 10) and it corresponded to Co-O in cobalt oxide. The Raman analyses (Fig. 10) of the used catalysts obtained under oxygen richer environments (*i.e.* C:O ratios of 8:2, 8:3 and 8:4) showed the presence of cobalt molybdate only (peak at ~ 937 cm^{-1}). These results indicate that the catalyst maintains its phase during the reaction as long as there is sufficient oxygen to re-oxidize the catalyst and maintain the initial phase (*i.e.* cobalt molybdate).

4 Summary and Conclusion

The cobalt molybdate catalyst synthesised by the co-precipitation method consisted of a mixture of the β- and α-$CoMoO_4$ phases, however, the catalyst was dominated by the β-$CoMoO_4$ phase and this is the more stable phase of cobalt molybdate. The TPR/O/R/O/R results showed that the catalyst can undergo the redox cycle without undergoing any irreversible transformation. The catalyst was tested in the oxidative dehydrogenation of *n*-octane under different carbon to oxygen ratios (*i.e.* 8:0, 8:1, 8:2, 8:3 and 8:4). The catalyst showed low conversion under dehydrogenation conditions and this resulted in the complete segregation of the cobalt molybdate catalyst. However, introduction of oxygen to the system significantly improved the conversion and also the selectivity to aromatics, and the catalyst maintained the cobalt molybdate phase after the reaction. The highest selectivity to octene of ~55% was obtained at an 8:1 carbon to oxygen ratio at 450 °C, while the highest selectivity to aromatics was obtained at an 8:3 carbon to oxygen ratio at the same temperature. At low temperature (350 °C), conversion was low and octene formation was favoured at all carbon to oxygen ratios again shows octenes are primary products. There is a decrease in the yield of the octenes with increase in the oxygen content, which is accompanied by an increase in the yield of aromatics, cracked and COx products. This resulted in a decrease in the value-added product yields. Therefore, the best carbon to oxygen ratio for octenes production is an 8:1 C:O ratio, while for aromatics it is 8:3.

Acknowledgments

The authors are thankful to SASOL, the NRF and THRIP (grant number TP1208035643) for financial support, and the EM unit at UKZN for helping with the SEM analyses.

Notes and references

[a] *Catalysis Research group, School of Chemistry and Physics, University of KwaZulu-Natal, PO 54001, Durban, South Africa. Fax: +27-312603109; Tel: +27-312603107; E-mail: friedric@ukzn.ac.za*

† Electronic Supplementary Information (ESI) available: [SEM of $CoMoO_4$, Raman spectroscopy of used catalyst under dehydrogenation condition, selectivity breakdown of CO and CO_2 and XRD of used catalyst at different carbon to oxygen ratio]. See DOI: 10.1039/b000000x/

5 References

1. V. D. B. C. Dasireddy, S. Singh and H. B. Friedrich, *Appl. Catal., A: Gen.*, 2012, **421–422**, 58.
2. F. Cavani and F. Trifirò, *Appl. Catal., A: Gen.*, 1992, **88**, 115.
3. B. Pillay, M. R. Mathebula and H. B. Friedrich, *Appl. Catal., A: Gen.*, 2009, **361**, 57.
4. C. Téllez, M. Abon, J. A. Dalmon, C. Mirodatos and J. Santamaría, *J. Catal.*, 2000, **195**, 113.
5. A. de Lucas, P. Sánchez, F. Dorado, M. J. Ramos and J. L. Valverde, *Appl. Catal., A: Gen.*, 2005, **294**, 215.

6. K. A. Williams and L. D. Schmidt, *Appl. Catal., A: Gen.*, 2006, **299**, 30.
7. A. A. Lemonidou, *Appl. Catal., A: Gen.*, 2001, **216**, 277.
8. M. Machli, E. Heracleous and A. A. Lemonidou, *Appl. Catal., A: Gen.*, 2002, **236**, 23.
9. R. K. Grasselli, *J. Chem. Educ.*, 1986, **63**, 216.
10. J. D. Burrington, C. T. Hartisch and R. K. Grasselli, *J. Catal.*, 1983, **81**, 489.
11. J. D. Burrington, C. T. Hartisch and R. K. Grasselli, *J. Catal.*, 1984, **87**, 363.
12. D. Halvorson. K. Aykan, A. W. Sleight, D. B. Rogers, *J. Catal.*, 1975, **35**, 401.
13. A. Mazurkiewicz. B. Grzybowska, J. Sloczinsky, *Appl. Catal., A: Gen.*, 1985, **13**, 223.
14. G. L. Schrader. U. Ozkan, *J. Catal.*, 1985, **95**, 120.
15. C. Martin. S. R. G. Carrazan, V. Rives, R. Vidal, *Appl. Catal., A: Gen.*, 1996, **135**, 95.
16. A. Kaddouri, R. Del Rosso, C. Mazzocchia, P. Gronchi and D. Fumagalli, *J. Therm. Anal. Calorim.*, 2001, **66**, 63.
17. B. Pillay, M. R. Mathebula and H. B. Friedrich, *Catal. Lett.*, 2011, **141**, 1297.
18. J. M. J. G. Lipsch and G. C. A. Schuit, *J. Catal.*, 1969, 15, 163.
19. Z. M. George, *J. Catal.*, 1974, **32**, 261.
20. Y. S. Yoon, W. Ueda and Y. Moro-oka, *Top. Catal.*, 1996, **3**, 265.
21. Y. S. Yoon, N. Fujikawa, W. Ueda, Y. Moro-oka and K. W. Lee, *Catal. Today*, 1995, **24**, 327.
22. L. A. Palacio, A. Echavarría, L. Sierra and E. A. Lombardo, *Catal. Today*, 2005, **107–108**, 338.
23. D. L. Stern and R. K. Grasselli, *J. Catal.*, 1997, **167**, 550.
24. J. Vila, F. Sapina, E. Martinez, V. Cortes and J. Podobinski, *Contrib. Sci.*, 2008, **4**, 223.
25. K. H. Jeziorowski, P. Grange, P. Gajardo, *J. Phys. Chem.*, 1980, **84**, 1825.
26. S. C. Chang, M. A. Leugers and S. R. Bare, *J. Phys. Chem.*, 1992, **96**, 10358.
27. J. L. Brito and A. L. Barbosa, *J. Catal.*, 1997, **171**, 467.
28. E. A. Elkhalifa and H. B. Friedrich, *Catal. Lett.*, 2011, **141**, 554.
29. E. A. Elkhalifa and H. B. Friedrich, *Appl. Catal., A: Gen.*, 2010, **373**, 122.
30. P. Meriaudeau, A. Thangaraj, C. Naccache and S. Narayanan, *J. Catal.*, 1994, **146**, 579.
31. B. C. Shi and B. H. Davis, *J. Catal.*, 1995, **157**, 626.
32. A. A. Lemonidou, G. J. Tjatjopoulos and I. A. Vasalos, *Catal. Today*, 1998, **45**, 65.
33. M. Narayanappa, V. D. B. C. Dasireddy and H. B. Friedrich, *Appl. Catal., A: Gen.*, 2012, 447–448, 135.
34. B. Solsona, J. M. López Nieto, P. Concepción, A. Dejoz, F. Ivars and M. I. Vázquez, *J. Catal.*, 2011, 280, 28.
35. V. D. B. C. Dasireddy, H. B. Friedrich and S. Singh, *Appl. Catal., A: Gen.*, 2013, 467, 142.